

Selective Reactivity and Oxidation of Dissolved Organic Matter by Manganese Oxides

Emma L. Trainer, Matthew Ginder-Vogel,* and Christina K. Remucal*



Cite This: *Environ. Sci. Technol.* 2021, 55, 12084–12094



Read Online

ACCESS |



Metrics & More



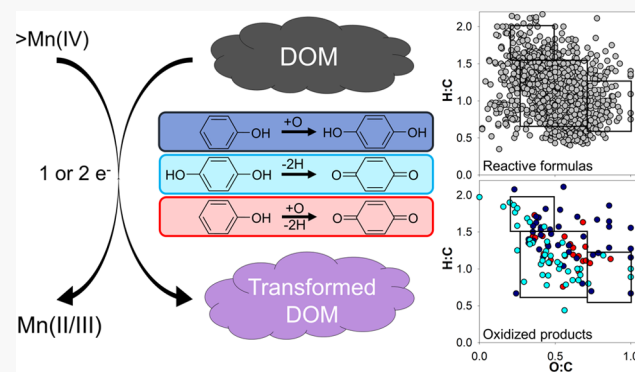
Article Recommendations



Supporting Information

ABSTRACT: Dissolved organic matter (DOM) varies widely across natural and engineered systems, but little is known about the influence of DOM composition on its reactivity with manganese oxides. Here, we investigate bulk and molecular transformations of 30 diverse DOM samples after reaction with acid birnessite (MnO_2), a strong oxidant that may react with DOM in Mn-rich environments or engineered treatment systems. The reaction of DOM with acid birnessite reduces Mn and forms DOM that is generally more aliphatic and lower in apparent molecular weight. However, the extent of reaction depends on the water type (e.g., wastewater, rivers) and highly aromatic DOM undergoes greater changes. Despite the variability in reactivity due to the DOM composition, aqueous products attributable to the oxidation of phenolic precursors are identified in waters analyzed by high-resolution mass spectrometry. The number of matched product formulas correlates significantly with indicators of DOM aromaticity, such as double-bond equivalents ($p = 2.43 \times 10^{-4}$). At the molecular level, highly aromatic, lignin-like carbon reacts selectively with acid birnessite in all samples despite the variability in initial DOM composition, resulting in the formation of a wide range of aqueous products. These findings demonstrate that DOM oxidation occurs in diverse waters but also suggest that reactivity with acid birnessite and the composition of the resulting aqueous DOM pool are composition-dependent and linked to the DOM source and initial aromaticity.

KEYWORDS: manganese oxides, dissolved organic matter, phenols, oxidation



INTRODUCTION

Dissolved organic matter (DOM) is a complex mixture of thousands of individual molecules containing carbon, hydrogen, oxygen, and heteroatoms (e.g., nitrogen).^{1–3} DOM is heterogeneous across natural and engineered waters with differing reactive functional groups, molecular weights, and aromaticity.^{2,4–9} The DOM source (e.g., allochthonous vs autochthonous) and extent of environmental processing alter its composition,^{5,10–13} with implications for bioavailability, contaminant mobility,^{4,9,14–17} photochemical transformation,^{5,8,18} and reactivity with oxidants (e.g., chlorine).^{12,13,19–22}

Metal oxides composed of manganese(III/IV), hereafter referred to as manganese (Mn) oxides, are ubiquitous, redox active minerals that react with inorganic^{23–25} and organic compounds,^{26–33} including DOM.^{27,31,34–38} Reactions of DOM with Mn oxides have important implications for DOM composition and biogeochemical cycling in the subsurface and at the sediment–water interface. Additionally, DOM may compete with target contaminants in treatment systems using Mn oxides. However, the heterogeneous nature of DOM complicates our understanding of its interactions with Mn oxides. Throughout this article, we use the term “reactivity” to

collectively describe processes that alter the composition of DOM because there are many possible transformation pathways for functional groups within DOM (e.g., phenols). Sorption and oxidation are the most widely considered reactions due to the sorption capacity and strong oxidation potential of birnessite minerals (i.e., MnO_2).^{23,27,34,36,39,40} Current knowledge of the oxidation of organic compounds by Mn oxides suggests that sorption must occur prior to oxidation.^{27,30,34,41} After sorption to the Mn surface, phenols may be oxidized via one- or two-electron-transfer reactions to produce hydroquinone- or quinone-like oxidation products, while Mn(IV) reaction sites are reduced to Mn(III) or Mn(II) centers, respectively. The oxidized organic carbon molecule and reduced Mn cation may remain sorbed to the Mn mineral

Received: June 16, 2021

Revised: August 9, 2021

Accepted: August 11, 2021

Published: August 25, 2021



ACS Publications

© 2021 American Chemical Society

12084

<https://doi.org/10.1021/acs.est.1c03972>
Environ. Sci. Technol. 2021, 55, 12084–12094

surface and thus get removed from the DOM pool or desorb into solution.^{27,29,30}

Each of these potential interactions between DOM and Mn oxides alters the DOM pool and solid-phase Mn oxide chemistry. Sorption fractionates DOM because molecules with higher aromaticity or a higher molecular weight may be more likely to sorb and no longer remain in the aqueous phase.^{18,42,43} If electron transfer and product desorption then occur, transformed organic products will shift the average DOM composition toward more oxidized carbon while releasing reduced Mn(II/III) cations. Ligand stabilization of these aqueous Mn(II/III) cations can further fractionate DOM by forming non-filter-passing organic matter–Mn(II/III) colloids.^{31,34,37}

Despite the possibility for DOM fractionation and multiple reaction mechanisms, there is a lack of studies comparing transformations across different DOM sources to determine how composition influences reactivity with Mn oxides. Most research on this system focuses either on the changes in Mn structure and DOM sorption^{35,36,44} or on comparing Mn oxides reacted with DOM isolates and/or model compounds.^{34,45,46} Studies that include whole water DOM commonly seek to understand interactions with dissolved trace metals (e.g., Fe, Al).^{47–49} Due to the nature of these studies, changes in organic carbon are typically attributed to oxidation based on evidence of Mn reduction or small organic acid product formation.^{16,37,38} However, these studies do not provide conclusive proof that DOM oxidation occurs; therefore, it is challenging to apply their results to more complex systems or different DOM sources.

This study examines how DOM composition influences reactivity with MnO₂ using 30 diverse whole waters under environmentally relevant conditions. We combine bulk DOM analyses (e.g., UV–vis measurements) with high-resolution mass spectrometry and X-ray absorption near-edge spectroscopy (XANES) to link molecular transformation to potential bulk predictors of DOM reactivity and to identify specific molecular DOM oxidation products. Our results demonstrate that (1) DOM transformation by acid birnessite depends on DOM composition and correlates most strongly with measures of aromaticity, (2) oxidation occurs across diverse waters and wastewater effluents reacted with acid birnessite, (3) high-resolution mass spectrometry can be used to confirm the production of aqueous oxidized products, and (4) although reactivity is dependent on DOM composition, the same lignin-like, highly aromatic formulas react in each sample to form various transformation products.

MATERIALS AND METHODS

Materials. All chemicals were commercially available and used as received. Acid birnessite was synthesized as described previously (specific surface area: $59 \pm 4 \text{ m}^2/\text{g}$).^{26,50} For more information, see the Supporting Information, Section S1.

Sampling. A total of 30 water samples were collected from sites with a wide range of DOM compositions across Wisconsin and Minnesota between 2017 and 2019 (Section S2). All waters were filtered (0.22 μm nylon) within 24 hours of collection and stored in amber glass bottles at 4 °C to prevent microbial growth. Waters were re-filtered prior to reactions.

Wastewater samples were collected from two separate sanitation districts. WW1 is the final effluent treated by disinfection and dechlorination from a treatment plant that

receives a large fraction of industrial wastewater. Samples from the second treatment plant, which treats primarily municipal wastewater, include the secondary effluent (WW2), the final effluent after UV disinfection (WW3), and a sample immediately downstream of effluent release (WW4).

Freshwaters included rivers (R), bogs (B), or lakes; lakes were categorized by their trophic status as oligotrophic (O), mesotrophic (M), or eutrophic (E).^{18,51,52} Surface grab samples were collected at least 1 m from the shore. Waters from the Madison, WI area include R1–R4 from the Yahara River and Badfish Creek and lakes E1–E3. Waters collected from rural Wisconsin include M1–M2 and E4 as well as O1–O4, B1–B2, and M3; the latter seven lakes are core sites in the North Temperate Lakes-Long Term Ecological Research (NTL-LTER) program.⁵³ Samples R5–R8 were collected from the St. Louis River in MN, along with E5–E7 and O5 sampled from the barrier peninsula separating Superior Bay and Lake Superior, respectively (Table S1 and Figure S1).

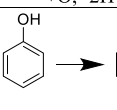
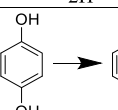
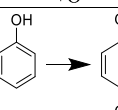
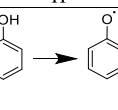
Water Chemistry. Water samples were characterized for dissolved organic carbon concentrations ([DOC], GE Sievers M5310C), trace metal and cation content by inductively coupled plasma-optical emission spectroscopy (Agilent 5110 VDV), and anion content by ion chromatography (Dionex ICS-2100). Ultraviolet–visible spectroscopy (Shimadzu 2401PC Spectrophotometer) was used to measure specific ultraviolet absorption (SUVA₂₅₄), which is equal to the absorbance at 254 nm divided by [DOC] and is related to DOM aromaticity as measured by ¹³C NMR.⁵⁴ Similarly, we measured E₂:E₃, or the ratio of absorbance at 250 to 365 nm, which is inversely related to direct measurements of molecular weight.^{8,55–57} While parameters like SUVA₂₅₄ and E₂:E₃ are commonly reported and can be used to investigate how DOM composition changes after reaction, it is important to note that UV–vis spectroscopy only detects DOM molecules that absorb light and can be influenced by species (e.g., iron, nitrate) that absorb light at low wavelengths.⁵⁸ Details on water chemical measurements are available in Section S2.

Reactions. This study includes three sets of reactions: a kinetic study of WW1 transformation to determine reaction timing (Section S3), examination of Mn and bulk DOM changes in 30 unique waters reacted with acid birnessite for 50 hours and 28 days (Section S4), and molecular characterizations of 14 representative waters preceding and following 50 hour reactions with acid birnessite (Table S5).

Reactions were buffered by 10 mM NaHCO₃[–] in addition to initial alkalinity at pH 7.0 ± 0.5 . The carbonate buffer has minimal interactions with both Mn oxides³⁰ and organic carbon quantification and is ubiquitous in natural waters.⁵⁹ All reactions were conducted in sealed sacrificial reactors with no headspace to prevent atmospheric exchange of CO₂; pH remained within 0.5 pH units of initial values after experiments.

Waters with [DOC] above 9 mg-C L^{–1} were diluted to $9.0 \pm 0.4 \text{ mg-C L}^{-1}$ (0.75 mM C) and reacted with 90 mg L^{–1} acid birnessite (1.05 mM Mn). Waters with lower [DOC] were reacted with a proportional concentration of acid birnessite to preserve the 3:4 C:Mn molar ratio, which was chosen to represent [DOC] and Mn concentrations in Mn-rich environments (e.g., lake sediment–water interfaces) where high reactivity is expected.⁶⁰ Reactors were stirred at 350 rpm under dark conditions. After 50 hours and 28 days, sacrificial reactors were filtered (0.22 μm nylon) to remove particulate Mn, which was air-dried at room temperature (22 ± 2 °C) for

Table 1. Tested Phenol Oxidation Pathways and Expected Molecular Changes for Each Reaction

Pathway	Phenol → benzoquinone	Hydroquinone → benzoquinone	Phenol → hydroquinone	Hydrogen Abstraction
Change	+O, -2H	-2H	+O	-H
Reaction				
$\Delta H/C$	-0.333	-0.333	0	-0.167
$\Delta O/C$	0.167	0	0.167	0
ΔDBE	1	1	0	0.5
ΔMW	+13.9792645	-2.01565006	+15.9949146	-1.00782503

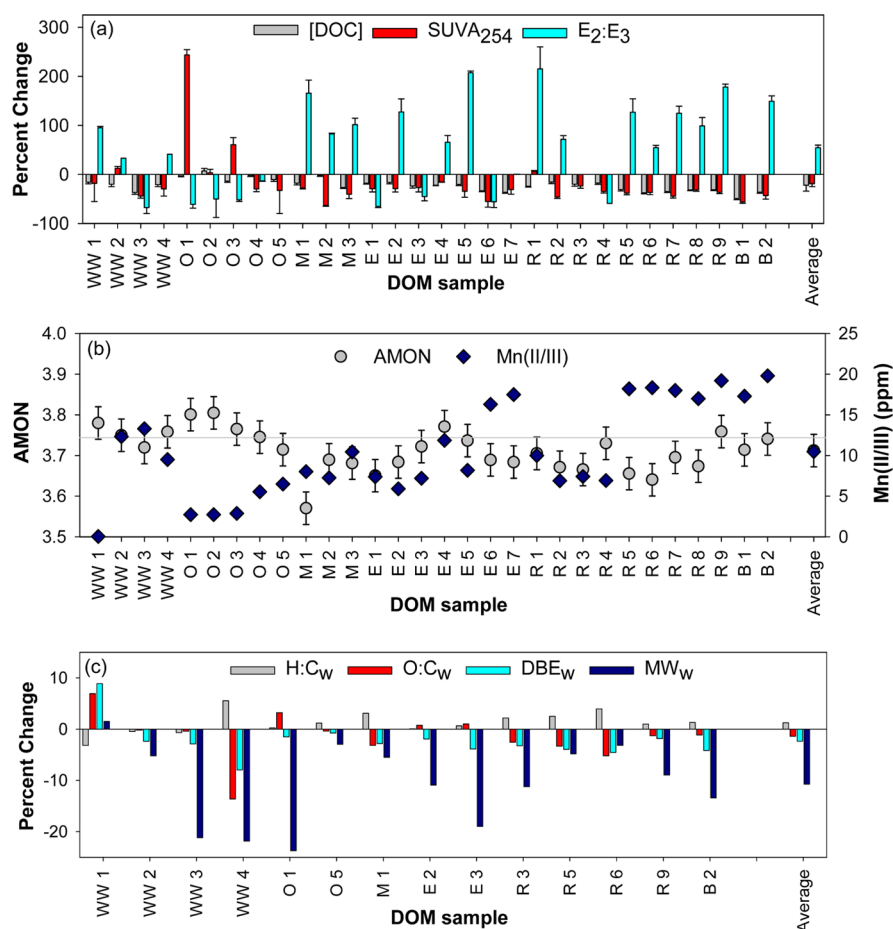


Figure 1. Percent changes in (a) [DOC], specific UV absorbance (SUVA₂₅₄), and E₂:E₃; (b) aqueous Mn(II/III) and average manganese oxidation number; and (c) weighted averages of H:C, O:C, DBE, and MW determined using high-resolution mass spectrometry following 50 h reactions of DOM with acid birnessite (3:4 C:Mn molar ratio, pH 7). Plot (b) includes a line marking the AMON of 3.74 for the acid birnessite starting material. Average changes across all waters are included as the final point on each plot to visualize overall reactivity trends. Percent changes from plots (a,c) are given in Table S6. Error bars represent (a) standard deviation of triplicate measurements and (b) standard deviation of triplicate Mn(II/III) measurements and AMON linear combination fitting method error described by Manceau et al.⁶¹

solid-phase analysis. Analogous control experiments were conducted in the absence of acid birnessite to determine DOM stability.

Filtered particulate average manganese oxidation number (AMON) was measured by quick scanning XANES (Q-XANES) analyzed using linear combination fitting.⁶¹ Filtrates were analyzed for [DOC], SUVA₂₅₄, E₂:E₃, and aqueous Mn(II/III) concentrations as described above.

Mass Spectrometry Analysis. The molecular composition of DOM in 14 waters was analyzed before and after reaction with acid birnessite by Fourier transform-ion cyclo-

tron resonance mass spectrometry (FT-ICR MS; Bruker Solarix XR 12T). These waters were selected to represent a range of water types and DOM compositions (Table S5). Organic matter was extracted from filtrates (250 mL) by solid-phase extraction (SPE; Agilent PPL; average [DOC] recovery: 58 ± 6%).⁶² Following negative electrospray ionization and FT-ICR MS analysis from 200 to 1000 *m/z*, *m/z* ions were converted to neutral masses, calibrated using common DOM formulas, and assigned formulas in R.^{5,12,13} Formula matches using the boundaries of C₁₋₁₈₀¹³C₀₋₁H₁₋₁₄₀O₀₋₈₀N₀₋₁S₀₋₁ were required to be within <0.5 ppm mass error and fall

within a homologous series (O vs CH₄ or +CH₂).⁶³ Details on sample preparation, FT-ICR MS analysis, formula matching, and calculations are provided in Section S5.

Relative intensities were calculated for each assigned *m/z* peak by dividing absolute peak intensities by the total intensity of all identified formulas within each sample. Weighted averages of H:C (H:C_w; unitless), O:C (O:C_w; unitless), molecular weight (MW_w; g/mol), and double-bond equivalents (DBE_w; unitless) were calculated using relative intensity.^{5,8,12,13,18,64} Samples were grouped by principal component analysis (PCA) using the relative intensities of identified formulas in each control and treated sample (Section S5).

Further analysis of FT-ICR MS results was based on relative intensity changes and formula presence/absence between the control and treated samples.¹³ Oxidation products were identified using expected mass changes for the oxidation of phenolic precursors to quinone-type products (i.e., -H, -2H, +O, +O/-2H; Table 1). Possible product masses were determined for each matched formula in control samples and then cross-checked against matched formulas in control and treated samples to identify unique products.

RESULTS AND DISCUSSION

Bulk DOM and Mn Oxide Transformation. To investigate the influence of DOM composition on reactivity, we reacted acid birnessite with 30 waters ranging in DOM composition (Table S2) and chemistry (Tables S3 and S4).^{5,64,65} These variations are the result of environment-specific factors, including differences in organic matter source, extent of environmental processing, and waterbody type (Section S2). Studies of DOM isolates, model compounds, and single DOM samples reacted with Mn oxides provide contradictory results. For instance, some studies report little sorption to the Mn oxide surface,^{45,46} while others report extensive sorption and fractionation,^{34,36,37,39,66,67} with varying transformation products^{16,36} and extent of reductive Mn oxide dissolution.^{16,29,35,39,67–69} Based on these studies, DOM composition is expected to influence the extent and manner of bulk DOM changes among the 30 waters. Specifically, we hypothesize that aromatic DOM from bogs and rivers will have greater changes in [DOC], SUVA₂₅₄, E₂:E₃, and Mn chemistry than less aromatic, microbially processed DOM from lakes because aromatic moieties (e.g., phenols) have greater sorption capacities and can be redox-active.

To test this hypothesis, changes in [DOC], SUVA₂₅₄, E₂:E₃, AMON, and aqueous [Mn] are analyzed for the first 50 hours of reaction based on initial kinetic experiments up to 50 hours with WW1 (Section S3); this sample was selected based on previous reports of lower reactivity in wastewater effluents than surface waters.⁵ These reactions were repeated for 28 days to quantify long-term transformation of bulk DOM and Mn; general trends discussed here are the same for the 50 hour and 28 day reactions (Section S4).

Across all 30 waters, [DOC] decreases by an average of 22 ± 12% after 50 hour reactions (Figure 1a). The average [DOC] loss is within the reported range of 5–40% loss across various DOM sources (e.g., forest leachates, commercial isolates, model organic acids) and Mn mineralogy (e.g., Mn-coated sands, birnessite).^{34–38,45} In this system, sorption to the mineral surface, mineralization to CO₂, or the formation of non-filter-passing Mn(II/III) colloids could contribute to [DOC] loss. Determining the route(s) of [DOC] loss in

these waters is beyond the scope of this study. However, sorption and colloid formation are the most likely mechanisms based on previous studies which use a combination of diffraction, X-ray photoelectron spectroscopy, electron microscopy, and XANES to confirm that both sorption^{4,34,36–38,45} and colloid formation can occur.^{4,35,44,47}

The bulk composition of DOM measured using UV–vis spectroscopy changes after 50 hours for all 30 waters (Figure 1a). In 25 waters, SUVA₂₅₄ decreases by an average of 1.1 ± 0.5 L mg-C⁻¹ m⁻¹ (36 ± 11%), which indicates either transformation of aromatic formulas or their selective sorption to the Mn surface. Given observations that phenols, anilines, and other aromatic organic compounds are highly reactive with MnO₂^{13,20,27,30} and are present in DOM,¹⁴ both mechanisms are plausible explanations for the decreasing SUVA₂₅₄ values and likely coexist. Decreases in [DOC] across all samples support the possibility of sorption to the Mn surface since this process physically removes DOM from the solution, while evidence for oxidation at the molecular level (i.e., a redox reaction that produces new oxidized products) is discussed below. SUVA₂₅₄ increases in five waters (O1, O2, O3, WW2, and R1) by an average of 0.9 ± 1.2 L mg-C⁻¹ m⁻¹ (65 ± 102%), indicating an increase in the bulk aromaticity of DOM during reaction of these samples with MnO₂ (Figure 1a), contrary to previous reports and the other 25 waters. The reason for this divergent trend is not clear based on bulk measurements since these samples include three different water types and other waters within the same category (e.g., all wastewaters) or from the same watersheds do not undergo the same changes.

E₂:E₃ values increase by an average of 4.7 ± 3.8 (108 ± 60%) in 21 waters, indicating a decrease in apparent molecular weight of DOM. In contrast, E₂:E₃ values decrease by an average of 2.1 ± 1.2 (52 ± 17%) in nine waters (O1, O2, O3, O4, E1, E3, E6, R4, and WW3), while E₂:E₃ in sample E7 does not change (Figure 1a). Previous studies note decreasing molecular weight after DOM reacts with Mn oxides, providing evidence for both molecular transformation and/or selective sorption of higher-molecular-weight compounds.^{34,36–38,45} For example, Fourier transform-infrared spectroscopy (FT-IR) analyses suggest that low-molecular-weight carbonyls form during the reaction of a natural organic matter isolate with sodium birnessite,⁴⁵ corresponding to an increase in E₂:E₃ and providing evidence of DOM transformation. Additionally, high-molecular-weight and aromatic DOM selectively sorbs to birnessite-coated sands and δ-MnO₂ based on high-pressure size exclusion chromatography analysis of three river DOM fractions.³⁴ Thus, these changes in bulk measures of molecular weight can be attributed to both transformation and/or sorption, suggesting that molecular evidence is necessary to confirm oxidation processes.

Increases in aqueous Mn(II/III) and decreases in AMON are indirect indicators of DOM oxidation. In this study, filter-passing Mn concentrations after 50 hour reactions with acid birnessite are as high as 20 ppm, which suggests that acid birnessite is reduced and forms dissolved Mn(II/III) (Figure 1b). However, visible particles form in all waters 24 hours after filtration, which we attribute to the formation of organic matter-bound Mn colloids that slowly precipitate after the reaction ends. After re-filtering the samples to remove these particles, dissolved Mn is below the detection limit (10 ppb) in all samples. The particles collected after 24 hours have an AMON of 2.64 ± 0.18 (Figure S5), which is consistent with

Mn(II/III) production and DOM oxidation. Furthermore, modeling with Visual MINTEQ⁷⁰ confirms that rhodochrosite is undersaturated in this system and these particles are colloidal forms of Mn(II/III). Previous studies also observe colloidal organic matter–Mn(III) formation using a combination of diffraction, XANES, X-ray photoelectron spectroscopy, and electron microscopy^{4,35,44,47,71} and note that Mn oxide AMON, aqueous cation content, and DOM aromaticity increase colloid aggregation.^{4,22,35,47} Thus, the concentration and AMON of particles forming within 24 hours in the reaction filtrate provide evidence of Mn reduction and colloid formation in this system as observed previously.

The average manganese oxidation number (AMON; i.e., the average oxidation state of Mn) of the remaining solid Mn oxide decreases significantly in four waters (E1, M1, R5, and R6) from the initial value of 3.74 ± 0.04 to 3.63 ± 0.04 ($p = 0.008$). For these samples, the decrease in AMON is consistent with Mn reduction and concurrent DOM oxidation. For the other 26 waters, AMON does not change (average 3.73 ± 0.04). The slight AMON changes are not surprising given the low C:Mn ratio, as well as desorption of reduced Mn discussed above. The changes in AMON and Mn(II/III) particle concentration are related; reactions with larger AMON decreases generally have more Mn(II/III) in the initial filtrate and more net reduction (Figure S6) than waters with minimal AMON changes. These trends also cluster by water type; DOM from oligotrophic lakes results in minimal AMON reduction and Mn(II/III) formation, while DOM from rivers results in greater AMON reduction and higher dissolved Mn(II/III) concentrations (Figure 1b).

Impact of DOM Composition and Water Chemistry on Reactivity. While changes in bulk DOM composition and Mn oxide transformation are similar across most of the studied waters, the extent of change differs and a small number of samples diverge from the overall trends (Table S6). In most cases, we observe slight decreases in [DOC], increases in $E_2:E_3$, decreases in $SUVA_{254}$, and little to no change in solid-phase AMON (Figure 1a,b). These changes are observed in DOM from mesotrophic lakes, bogs, and rivers, as well as 4 of the 7 eutrophic lakes and 2 of the 4 wastewaters (i.e., 20 out of 30 waters). In contrast, $E_2:E_3$ decreases in all five oligotrophic lakes and $SUVA_{254}$ increases in three of the five oligotrophic lakes. These five oligotrophic lakes, along with WW1, also have the lowest measured [Mn(II/III)], suggesting minimal Mn reduction (Figure S6). The trends among waters indicate that the reactivity of more aromatic DOM (e.g., from bogs) is consistent with DOM oxidation or preferential sorption of aromatic molecules, while DOM that is less aromatic and more microbially processed (e.g., oligotrophic lakes and wastewater effluents) may react through different mechanisms.

The influence of the water source on changes in bulk DOM is supported by linear regression analysis (Table S7). We compare changes in DOM and Mn bulk measurements with initial $SUVA_{254}$ and $E_2:E_3$ values to assess how aromaticity and apparent MW impact reactivity. Initial $SUVA_{254}$ values negatively correlate with percent changes in $SUVA_{254}$ ($p = 0.006$) and positively correlate with percent changes in both $E_2:E_3$ ($p = 0.004$) and reduced [Mn(II/III)] ($p = 0.001$). These significant correlations suggest that DOM with greater initial $SUVA_{254}$ values will have larger decreases in $SUVA_{254}$ and increases in $E_2:E_3$ and aqueous [Mn] during reaction with Mn oxides, supporting our observation that more aromatic DOM is more reactive. In contrast, initial $E_2:E_3$ values only

significantly correlate with percent changes in $E_2:E_3$ ($p = 0.047$), indicating that apparent molecular weight of DOM is not a major predictor of its reactivity. Furthermore, although sulfate and ionic strength may influence the reactivity of manganese oxides^{66,72–74} and DOM,^{15,19,22,48,49,75} they are not correlated with measured parameters in these samples.

Changes in solid-phase AMON are not significantly correlated with any of the tested bulk parameters (Table S7), although this is not surprising given that many waters had final solid-phase AMON values within error of the starting material. However, the four waters with AMON reduction have initial $SUVA_{254}$ values greater than $2.6 \text{ L mg}^{-1} \text{ m}^{-1}$. This provides further evidence of quantifiable Mn reduction and therefore DOM oxidation after reaction with aromatic DOM, as expected based on the high reactivity and oxidation potential of electron-rich phenolic moieties.^{13,14,20,34,36}

The changes in optical parameters and net Mn reduction observed in most DOM samples demonstrate that the composition of DOM changes due to reaction with acid birnessite. Although these trends may be attributable to DOM oxidation, bulk measurements alone cannot demonstrate that oxidation is the primary mechanism of transformation rather than selective sorption and colloid formation. Furthermore, a subset of waters do not follow the trends in bulk DOM and Mn changes exhibited by most waters in this data set (Table S6). These opposing transformations demonstrate the complexity of DOM reactions with Mn oxides that can only be captured with diverse samples, such as those included in this study, and require molecular-level analysis to confirm oxidative transformations.

Molecular Transformations Analyzed by FT-ICR MS. A total of 14 waters which represent the range of 50 h changes in apparent aromaticity, molecular weight, and Mn reduction (Table S6) are analyzed with FT-ICR MS analysis to determine how reaction with acid birnessite alters DOM composition and to obtain evidence of DOM oxidation. While the SPE material used in this study is ideal for isolating the fraction of DOM that is detected by FT-ICR MS,⁷⁶ this technique is selective because only molecules that are retained by SPE and that ionize using negative mode electrospray ionization are detected. Despite this limitation, FT-ICR MS enables specific analyses of molecular changes in DOM. Some parameters (e.g., $H:C_w$, DBE_w) provide alternative methods to quantify changes in aromaticity, whereas other parameters (e.g., $O:C_w$) provide oxidation state measurements that are not possible with bulk measurements. Additionally, the formulas assigned after FT-ICR MS analysis can be used to identify products of specific reactions, notably oxidation of phenolic moieties.¹³

In the initial samples, 4585 ± 611 formulas are identified by FT-ICR MS on average, which are visualized in van Krevelen diagrams (Section S7 and Figure S10). Most of the identified formulas contain only C, H, and O ($52 \pm 7\%$), with variable amounts of N- ($35 \pm 3\%$) and S-containing formulas ($13 \pm 10\%$; Table S9). The initial DOM composition varies widely among samples with $H:C_w$ values ranging from 1.11 to 1.42, $O:C_w$ from 0.41 to 0.54, and DBE_w from 6.81 to 10.09 (Table S10). The number of identified formulas decreases in all 14 samples after reaction with acid birnessite with an average loss of 268 CHO formulas (11%), 230 CHON formulas (14%), and 87 CHOS formulas (14%; Table S9), indicating no preferential removal of heteroatom-containing formulas.

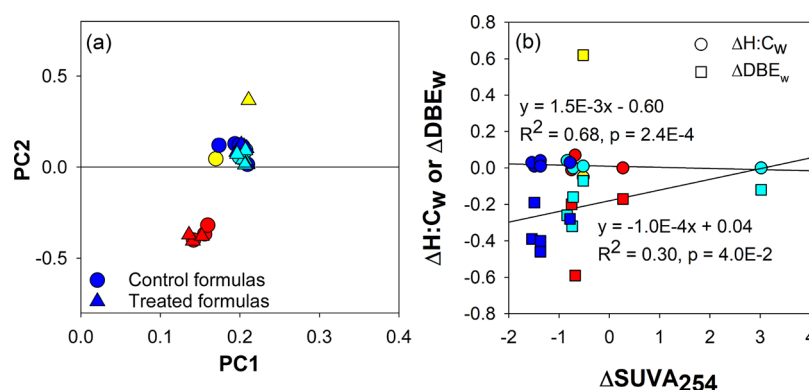


Figure 2. PCA plots of (a) relative formula intensities of both control and treated waters. The variances explained by PC1 and PC2, respectively, are 77.6 and 11.7%. (b) Changes in bulk UV–vis measurements versus molecular FT-ICR MS measurements which represent changes in organic matter aromaticity, H:C_w , and DBE_w versus SUVA_{254} . Points correspond to wastewater 1 (WW1; yellow), other wastewaters (WW2–4; red), bogs and rivers (blue), and lakes (cyan).

PCA using formula intensities in control and treated samples is used to differentiate between DOM compositions at the molecular level. PCA reveals four clusters of samples: WW1, WW2–4, lakes, and rivers and bogs (Figure S8). These groupings suggest significant differences in the molecular composition of DOM in these samples both before and after reaction with acid birnessite. Notably, the reacted samples cluster near their controls (Figure 2a), suggesting that differences among reacted samples are largely driven by initial DOM composition. The distances between control and treated samples are a proxy measure for the extent of reaction with acid birnessite,⁷⁷ and while PCA distance does not correlate significantly with other water characteristics (Table S8), this metric suggests that WW2, WW3, and WW4 undergo the least change during reaction, natural waters undergo moderate changes, and WW1 has the greatest transformation with acid birnessite (Figure S9). These PCA results confirm that definitive delineations exist between water types as observed in the bulk characteristics and support our hypothesis that reactivity in this system depends on DOM composition (Figures 1 and 2a).

Changes in weighted averages derived from FT-ICR MS data provide additional insight into overall DOM reactivity with acid birnessite. H:C_w increases by 1.2% and DBE_w decreases by 2.4% on average (Figure 1c), which are consistent with decreasing aromaticity and the observed average decrease in SUVA_{254} (Figure 2b). MW_w decreases by 10.7% on average, in agreement with the general increase in $\text{E}_2:\text{E}_3$ (Figure S7 and Table S6). Inconsistent changes in MS-derived measures of aromaticity and apparent molecular weight are observed in WW1, WW2, and WW3, although the magnitudes of decreases in H:C_w or increases in DBE_w are small.

Collectively, these results provide insight into how the initial composition of DOM impacts its reactivity with Mn oxides. The wastewater samples cluster separately from the natural water samples by PCA (Figure 2a), suggesting that there is a molecular basis for the differential reactivity observed in this type of DOM. For example, the FT-ICR MS results indicate that most wastewater samples (i.e., WW2–WW4) are less reactive than natural DOM samples (Figure S9), in agreement with our observation that less aromatic DOM is less reactive based on linear relationships using bulk and MS measurements of aromaticity (i.e., initial SUVA_{254} and H:C_w ; Tables S7 and S8). However, WW1 is an outlier in many quantitative

measures with decreasing H:C_w and increasing O:C_w , DBE_w , and MW_w values (Figure 1) and is molecularly distinct from the other wastewater samples (Figure 2a), which we hypothesize is due to the high percentage of the industrial wastewater influent to this treatment plant. The variable reactivity across DOM samples highlights the importance of using a wide range of whole waters to study DOM transformation, rather than focusing on a single sample. Additionally, the use of multiple techniques to investigate changes in this complex matrix and general agreement between UV–vis and FT-ICR MS measurements (Figures 2b and S7) supports the conclusion that on average, DOM remaining in the aqueous phase becomes less aromatic and lower in molecular weight upon reaction with acid birnessite. It is noteworthy that UV–vis and FT-ICR MS reveal similar trends because each of these techniques only captures a portion of the DOM pool (i.e., molecules that absorb light and ionize in the negative mode, respectively).

O:C_w is a measure of the oxidation state of formulas detected by FT-ICR MS and does not align with any presented bulk measurements. Because MnO_2 reacts with phenolic compounds by adding oxygen to the phenolic moiety (Table 1)^{26–30,32} and phenols are important functional groups in DOM,^{1,2,13,17,18,20,78–80} we expect that O:C_w would increase in DOM after reaction. However, O:C_w only increases in 4 of the 14 waters by an average of 2.1% and decreases in the remaining 10 samples by 1.9% on average (Tables S6 and S10). Thus, DOM remaining in solution is slightly reduced relative to the initial DOM, contradicting FT-IR observations of reacted DOM,^{34,35,37} as well as measures of Mn reduction in this data set and previous literature studies.^{4,24,34,35} However, weighted values encompass all transformations to the DOM pool including non-oxidative reactions and fractionation due to selective sorption and colloidal organic matter–Mn(II/III) formation. Studies using a fulvic acid isolate or DOM derived from biochar have similarly observed that O:C_w can either increase or decrease after reaction with Mn oxides.^{81,82} While decreases in O:C_w indicate reduction of C in the bulk DOM pool, this result does not negate other measures of aromaticity and molecular weight which suggest that oxidation occurs. Rather, more specific evidence supporting the formation of oxidized product formulas is necessary.

Oxidation Product Formulas. To determine whether oxidation occurs on a molecular level in the DOM samples

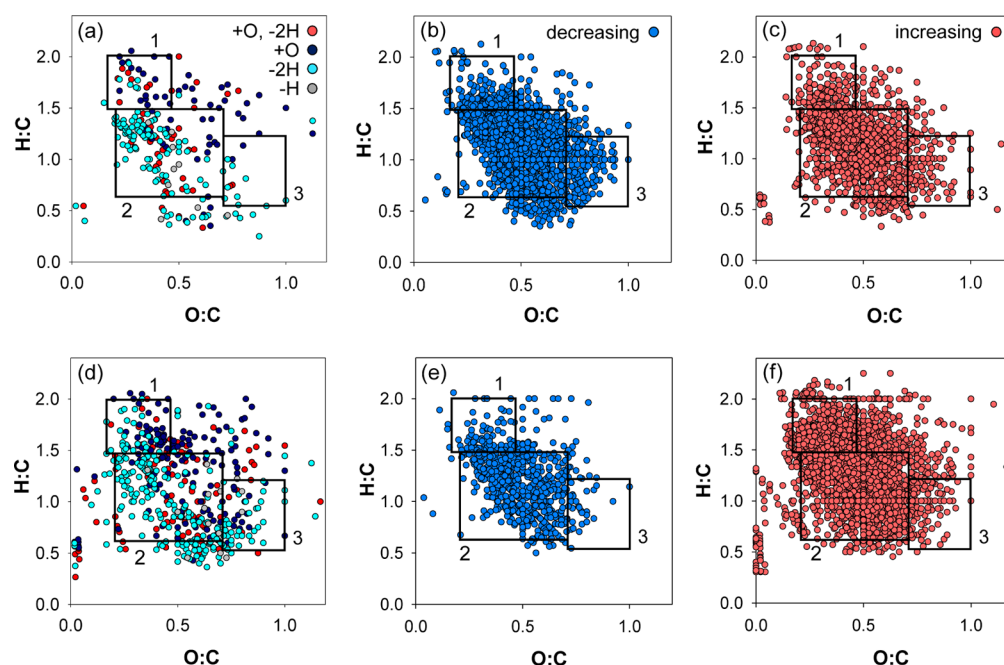


Figure 3. van Krevelen diagrams showing changes in St. Louis River (R6; a–c) and Western Lake Superior Sanitary District effluent (WW1; d–f) DOM formulas after 50 hour reactions with acid birnessite. (a,d) Matched phenol oxidation and hydrogen abstraction products formed by phenolic oxidation pathways listed in Table 1, (b,e) formulas which decrease in intensity during reaction, and (c,f) formulas which increase in intensity during reaction. The overlaid boxes indicate (1) protein-like, (2) lignin-like, and (3) tannin-like formulas.¹ van Krevelen diagrams for the other 11 waters are in Figures S11–S14.

despite contradictory $O:C_w$ results, matched FT-ICR MS formulas are analyzed for potential oxidation products. Transformation of phenol to hydroquinone or benzoquinone (Table 1) are common oxidation pathways of reactive aromatic moieties in DOM^{13,19,20} and are likely to occur in this system as phenolic compounds are highly reactive with MnO_2 .^{27,29,30} Three possible oxidation pathways are tested: phenol to hydroquinone (+O), hydroquinone to benzoquinone (−2H), and phenol to benzoquinone (+O and −2H), as well as hydrogen abstraction (−H) as an alternate rate-limiting pathway of phenol oxidation (Table 1).^{30,83,84} Identified unique product formulas are compared to potential oxidized products determined from the original control formula masses plus or minus the specific molecular weight changes corresponding to phenol oxidation. The resulting mass lists are compared to the matched control formulas to ensure that any resulting product formulas are unique to the treated samples. This analysis assumes that each initial DOM molecule could theoretically undergo a phenol-like reaction; it does not assume that all molecules present in DOM contain phenolic moieties.

Predicted products based on phenol oxidation mechanisms are identified in all 14 samples (Figure 3 and Table S11). These waters average 83 ± 48 phenol to hydroquinone, 88 ± 52 hydroquinone to benzoquinone, 78 ± 50 phenol to benzoquinone, and 6 ± 8 hydrogen abstraction products after reaction with acid birnessite. The limited number of hydrogen abstraction products suggests that this mechanism is possible but is less important for DOM transformation by acid birnessite in these waters. Sample WW1 has the most detected oxidation products (i.e., 687 in total; Figure 3d), which is notable as WW1 is a consistent outlier in DOM characteristic changes. Its increase in $O:C_w$ (Table S6) aligns with the large number of oxidized product formulas, while its trends of

decreasing $H:C_w$ and increasing MW_w are contrary to most other waters. The universal presence of oxidation products (Figure S11) confirms that oxidation occurs at the molecular level in all samples, even those with decreasing $O:C_w$ values or contrary bulk measurements (Figure 1).

The number of oxidation products formed across all waters correlates positively with percent changes in both DBE_w ($p = 7.6 \times 10^{-5}$) and MW_w ($p = 0.002$; Table S8). These trends suggest that waters which form more DOM oxidation products also increase in both MW and DBE , which is counter-intuitive based on expected decreases in molecular weight and aromaticity of the entire DOM pool.^{8,13,18} However, these trends are consistent with known reactions of individual phenols or hydroquinones (Table 1). Notably, no bulk DOM properties or solid-phase Mn changes correlate with the number of phenolic oxidation products, indicating that these measurements cannot be used as proxies for DOM oxidation of phenolic precursors.

This is the first, specific evidence of molecular oxidation products during the transformation of DOM by manganese oxides. The identified product formulas are not comprehensive as we match only phenolic oxidation pathways and other reactive DOM moieties may be oxidized in this system (e.g., anilines). Nonetheless, these results suggest that high-resolution formula identification can confirm specific oxidative transformations and provide conclusive evidence that oxidation occurs in the studied DOM samples.

Molecular Reactivity Trends. Despite the heterogeneous nature of the DOM in these waters, further analysis of FT-ICR MS data demonstrates that a common pool of formulas is most reactive with acid birnessite. We identify formulas that are unique to the control samples and treated waters (Figure S12), which are designated as completely reacted and unique product formulas, respectively. Formulas that react completely

with acid birnessite are primarily located in the lignin-like region, which is consistent with the oxidation of aromatic phenolic moieties,¹³ although protein-like formulas also react in some samples. Notably, many of the unique product formulas occupy similar regions on the van Krevelen diagram as the reacted formulas (Figure S12), which agrees with the modest changes observed in the weighted averages in these waters (Table S6).

Similar trends appear in van Krevelen diagrams of formulas which decrease or increase in relative intensity during reaction. As with the unique formulas, these plots are similar across all samples (Figures 3, S13, and S14). The reactive formulas fall in the same lignin-like region that contains aromatic, electron-rich phenolic moieties and has been linked to DOM reactivity with other oxidants including ozone^{13,21,84–86} and hydroxyl radical.^{5,12,13,18,20,21,78,84,86} The formulas which increase in intensity during reaction are widely distributed across the protein-, lignin-, and tannin-like regions (Figure S14), suggesting the possibility of different types of products and reaction mechanisms. Furthermore, the formulas that increase in relative intensity after reaction span a greater range of the van Krevelen diagram than the identified oxidation products, which are typically confined to the lignin-like region of the plots and are consistent with selective phenol-like reactions within the pool of DOM molecules (Figures 3 and S11). The scattered product formulas support the observed differences in aromaticity and molecular weight measures using both bulk measurements and FT-ICR MS analysis (Table S6) as well as evidence of non-oxidative transformations occurring in the DOM pool and are supported by observations made after reacting high concentrations (~ 300 mg-C L⁻¹) of Suwannee River fulvic acid with δ -MnO₂ at pH 4.⁴⁶ Although there are differences in bulk DOM compositional changes and a wide range of products are generated by the reaction of DOM and acid birnessite, these results demonstrate that MnO₂ reacts selectively with electron-rich, lignin-like formulas even in waters containing highly diverse DOM.

Environmental Implications. Organic matter oxidation is considered a primary transformation pathway by Mn oxides, and this study demonstrates, with molecular product identification, that oxidation selectively occurs with phenolic moieties in DOM regardless of the water source. We observe composition-dependent transformations to the bulk DOM pool, with oxidation products identified in all 14 waters analyzed by FT-ICR MS (Figure 3 and Table S11). DOM oxidation by Mn oxides is often assumed based on bulk results and theoretical reaction chemistry (e.g., Mn reduction)^{16,22,34–37,40,44,46,67,69,87–89} but was unsubstantiated with conclusive molecular evidence prior to this study. Furthermore, initial aromaticity, as measured by SUVA₂₅₄, H:C_w, and DBE_w, is the greatest control on extent of DOM transformation and correlates significantly with the number of oxidation products detected after reaction with acid birnessite (Table S8), suggesting that aromaticity may be the best predictor of extent of oxidation among natural waters. Future work should use organic matter derived from soils to investigate if these trends also occur in pedological systems.

Bulk DOM measures suggest that other transformation and organic matter removal pathways (e.g., sorption) occur alongside oxidation to alter the reacted aqueous DOM pool. [DOC] loss, reduced Mn colloid formation, and variability in bulk DOM transformation (e.g., apparent MW; Figure 1) indicate that oxidation is not the only mechanism altering

DOM and Mn in this system. These competing mechanisms necessitate further research to identify other DOM transformation mechanisms, to investigate the composition of sorbed organic matter, and to elucidate influential environmental parameters on both sorption and oxidation processes by manganese oxides.

The effects of these transformation mechanisms will impact our understanding and predictions of contaminant fate, bioavailability, and other dependent environmental processes. For example, organic matter was previously demonstrated to both enhance and inhibit contaminant degradation by MnO₂,^{22,23,27,36,38,40,89,90} although the mechanisms are unknown and may depend on DOM composition. Thus, this study provides the molecular framework and confirmation of oxidation necessary to investigate how DOM composition alters manganese oxide reactivity in complex environments.

■ ASSOCIATED CONTENT

Supporting Information

The Supporting Information is available free of charge at <https://pubs.acs.org/doi/10.1021/acs.est.1c03972>.

Additional details on materials, sampling locations, methods, water chemistry, kinetic experiments, and mass spectrometry analysis of all samples (PDF).

■ AUTHOR INFORMATION

Corresponding Authors

Matthew Ginder-Vogel – *Environmental Chemistry and Technology Program, University of Wisconsin—Madison, Madison, Wisconsin 53706, United States; Department of Civil and Environmental Engineering, University of Wisconsin—Madison, Madison, Wisconsin 53706, United States; orcid.org/0000-0001-9183-1931; Phone: (608) 262 0768; Email: mgindervogel@wisc.edu; Fax: (608) 262 0454*

Christina K. Remucal – *Environmental Chemistry and Technology Program, University of Wisconsin—Madison, Madison, Wisconsin 53706, United States; Department of Civil and Environmental Engineering, University of Wisconsin—Madison, Madison, Wisconsin 53706, United States; orcid.org/0000-0003-4285-7638; Phone: (608) 262 1820; Email: remucal@wisc.edu; Fax: (608) 262 0454*

Author

Emma L. Trainer – *Environmental Chemistry and Technology Program, University of Wisconsin—Madison, Madison, Wisconsin 53706, United States; orcid.org/0000-0002-0091-8028*

Complete contact information is available at: <https://pubs.acs.org/doi/10.1021/acs.est.1c03972>

Notes

The authors declare no competing financial interest.

■ ACKNOWLEDGMENTS

Funding was provided by the National Science Foundation (CBET 1944464). The authors thank Stephanie Berg and Amber White for sampling assistance and Elizabeth Tomaszewski for recording XANES spectra of 28 day reaction solids. X-ray absorption spectroscopy was conducted at Sector 10 of the Advanced Photon Source and Sector 4 at the

National Synchrotron Light Source II. MRCAT operations are supported by the Department of Energy and MRCAT member institutions. This research used resources of the Advanced Photon Source, a U.S. Department of Energy (DOE) Office of Science User Facility operated for the DOE Office of Science by Argonne National Laboratory, under Contract no. DE-AC02-06CH11357 and the XFM Beamline of the National Synchrotron Light Source II, a U.S. Department of Energy (DOE) Office of Science User Facility operated for the DOE Office of Science by Brookhaven National Laboratory, under Contract no. DE-SC0012704. The authors acknowledge the UW-Madison Human Proteomics Program Mass Spectrometry Facility (Wisconsin partnership funds; NIH S10OD018475) for support in obtaining FT-ICR MS data and Yanlong Zhu for assistance with the instrument. The authors also thank the Northern Temperate Lakes Long-Term Ecological Research Program (NSF DEB 1440297), Madison Metropolitan Sewerage District, and Western Lake Superior Sanitary District for sampling resources.

■ REFERENCES

- (1) Minor, E. C.; Swenson, M. M.; Mattson, B. M.; Oyler, A. R. Structural characterization of dissolved organic matter: A review of current techniques for isolation and analysis. *Environ. Sci. Processes Impacts* **2014**, *16*, 2064–2079.
- (2) Nebbioso, A.; Piccolo, A. Molecular characterization of dissolved organic matter (DOM): A critical review. *Anal. Bioanal. Chem.* **2013**, *405*, 109–124.
- (3) D'Andrilli, J.; Cooper, W. T.; Foreman, C. M.; Marshall, A. G. An ultrahigh-resolution mass spectrometry index to estimate natural organic matter lability. *Rapid Commun. Mass Spectrom.* **2015**, *29*, 2385–2401.
- (4) Aiken, G. R.; Hsu-Kim, H.; Ryan, J. N. Influence of dissolved organic matter on the environmental fate of metals, nanoparticles, and colloids. *Environ. Sci. Technol.* **2011**, *45*, 3196–3201.
- (5) Berg, S. M.; Whiting, Q. T.; Herrli, J. A.; Winkels, R.; Wammer, K. H.; Remucal, C. K. The role of dissolved organic matter composition in determining photochemical reactivity at the molecular level. *Environ. Sci. Technol.* **2019**, *53*, 11725–11734.
- (6) Dittmar, T. Reasons behind the long-term stability of dissolved organic matter. *Biogeochemistry of Marine Dissolved Organic Matter*; Academic Press, 2015; pp 369–388.
- (7) He, W.; Jung, H.; Lee, J.-H.; Hur, J. Differences in spectroscopic characteristics between dissolved and particulate organic matters in sediments: Insight into distribution behavior of sediment organic matter. *Sci. Total Environ.* **2016**, *547*, 1–8.
- (8) Maizel, A. C.; Remucal, C. K. Molecular composition and photochemical reactivity of size-fractionated dissolved organic matter. *Environ. Sci. Technol.* **2017**, *51*, 2113–2123.
- (9) Wagner, S.; Riedel, T.; Niggemann, J.; Vähätalo, A. V.; Dittmar, T.; Jaffé, R. Linking the molecular signature of heteroatomic dissolved organic matter to watershed characteristics in world rivers. *Environ. Sci. Technol.* **2015**, *49*, 13798–13806.
- (10) Bodhipaksha, L. C.; Sharpless, C. M.; Chin, Y.-P.; Sander, M.; Langston, W. K.; MacKay, A. A. Triplet photochemistry of effluent and natural organic matter in whole water and isolates from effluent-receiving rivers. *Environ. Sci. Technol.* **2015**, *49*, 3453–3463.
- (11) Chen, Y.; Hozalski, R. M.; Olmanson, L. G.; Page, B. P.; Finlay, J. C.; Brezonik, P. L.; Arnold, W. A. Prediction of photochemically produced reactive intermediates in surface waters via satellite remote sensing. *Environ. Sci. Technol.* **2020**, *54*, 6671–6681.
- (12) Bulman, D. M.; Remucal, C. K. Role of reactive halogen species in disinfection byproduct formation during chlorine photolysis. *Environ. Sci. Technol.* **2020**, *54*, 9629–9639.
- (13) Remucal, C. K.; Salhi, E.; Walpen, N.; von Gunten, U. Molecular-level transformation of dissolved organic matter during oxidation by ozone and hydroxyl radical. *Environ. Sci. Technol.* **2020**, *54*, 10351–10360.
- (14) Fimmen, R. L.; Cory, R. M.; Chin, Y.-P.; Trouts, T. D.; McKnight, D. M. Probing the oxidation–reduction properties of terrestrially and microbially derived dissolved organic matter. *Geochim. Cosmochim. Acta* **2007**, *71*, 3003–3015.
- (15) Gücker, B.; Silva, R. C. S.; Graeber, D.; Monteiro, J. A. F.; Boëchat, I. G. Urbanization and agriculture increase exports and differentially alters elemental stoichiometry of dissolved organic matter (DOM) from tropical catchments. *Sci. Total Environ.* **2016**, *550*, 785–792.
- (16) Polubesova, T.; Chefetz, B. DOM-affected transformation of contaminants on mineral surfaces: A review. *Crit. Rev. Environ. Sci. Technol.* **2014**, *44*, 223–254.
- (17) Subdiaga, E.; Orsetti, S.; Haderlein, S. B. Effects of sorption on redox properties of natural organic matter. *Environ. Sci. Technol.* **2019**, *53*, 14319–14328.
- (18) Maizel, A. C.; Li, J.; Remucal, C. K. Relationships between dissolved organic matter composition and photochemistry in lakes of diverse trophic status. *Environ. Sci. Technol.* **2017**, *51*, 9624–9632.
- (19) Wallace, G. C.; Sander, M.; Chin, Y.-P.; Arnold, W. A. Quantifying the electron donating capacities of sulfide and dissolved organic matter in sediment pore waters of wetlands. *Environ. Sci. Processes Impacts* **2017**, *19*, 758–767.
- (20) Walpen, N.; Getzinger, G. J.; Schroth, M. H.; Sander, M. Electron-donating phenolic and electron-accepting quinone moieties in peat dissolved organic matter: quantities and redox transformations in the context of peat biogeochemistry. *Environ. Sci. Technol.* **2018**, *52*, 5236–5245.
- (21) Wenk, J.; Aeschbacher, M.; Salhi, E.; Canonica, S.; von Gunten, U.; Sander, M. Chemical oxidation of dissolved organic matter by chlorine dioxide, chlorine, and ozone: Effects on its optical and antioxidant properties. *Environ. Sci. Technol.* **2013**, *47*, 11147–11156.
- (22) Zhang, S.; Gutierrez, L.; Niu, X.-Z.; Qi, F.; Croue, J.-P. The characteristics of organic matter influence its interfacial interactions with MnO₂ and catalytic oxidation processes. *Chemosphere* **2018**, *209*, 950–959.
- (23) Borch, T.; Kretzschmar, R.; Kappler, A.; Cappellen, P. V.; Ginder-Vogel, M.; Voegelin, A.; Campbell, K. Biogeochemical redox processes and their impact on contaminant dynamics. *Environ. Sci. Technol.* **2010**, *44*, 15–23.
- (24) Peña, J.; Kwon, K. D.; Refson, K.; Bargar, J. R.; Sposito, G. Mechanisms of nickel sorption by a bacteriogenic birnessite. *Geochim. Cosmochim. Acta* **2010**, *74*, 3076–3089.
- (25) Wang, Z.; Giammar, D. E. Metal contaminant oxidation mediated by manganese redox cycling in subsurface environment. In *Advances in the Environmental Biogeochemistry of Manganese Oxides*; Feng, X., Li, W., Zhu, M., Sparks, D. L., Eds; American Chemical Society: Washington, D.C., 2015; Vol. 1197, pp 29–50.
- (26) Balgooyen, S.; Alaimo, P. J.; Remucal, C. K.; Ginder-Vogel, M. Structural transformation of MnO₂ during the oxidation of bisphenol A. *Environ. Sci. Technol.* **2017**, *51*, 6053–6062.
- (27) Remucal, C. K.; Ginder-Vogel, M. A critical review of the reactivity of manganese oxides with organic contaminants. *Environ. Sci. Processes Impacts* **2014**, *16*, 1247–1266.
- (28) Shaikh, N.; Taujale, S.; Zhang, H.; Artyushkova, K.; Ali, A.-M. S.; Cerrato, J. M. Spectroscopic investigation of interfacial interaction of manganese oxide with triclosan, aniline, and phenol. *Environ. Sci. Technol.* **2016**, *50*, 10978–10987.
- (29) Stone, A. T. Reductive dissolution of manganese(III/IV) oxides by substituted phenols. *Environ. Sci. Technol.* **1987**, *21*, 979–988.
- (30) Trainer, E. L.; Ginder-Vogel, M.; Remucal, C. K. Organic structure and solid characteristics determine reactivity of phenolic compounds with synthetic and reclaimed manganese oxides. *Environ. Sci. Water Res. Technol.* **2020**, *6*, 540–553.
- (31) Wang, X.; Xiang, W.; Wang, S.; Ge, J.; Qu, R.; Wang, Z. Oxidative oligomerization of phenolic endocrine disrupting chemicals mediated by Mn(III)-L complexes and the role of phenoxyl radicals in

the enhanced removal: Experimental and theoretical studies. *Environ. Sci. Technol.* **2020**, *54*, 1573–1582.

(32) Pavitt, A. S.; Bylaska, E. J.; Tratnyek, P. G. Oxidation potentials of phenols and anilines: correlation analysis of electrochemical and theoretical values. *Environ. Sci. Processes Impacts* **2017**, *19*, 339–349.

(33) Salter-Blanc, A. J.; Bylaska, E. J.; Lyon, M. A.; Ness, S. C.; Tratnyek, P. G. Structure-activity relationships for rates of aromatic amine oxidation by manganese dioxide. *Environ. Sci. Technol.* **2016**, *50*, 5094–5102.

(34) Allard, S.; Gutierrez, L.; Fontaine, C.; Croué, J.-P.; Gallard, H. Organic matter interactions with natural manganese oxide and synthetic birnessite. *Sci. Total Environ.* **2017**, *583*, 487–495.

(35) Li, Q.; Xie, L.; Jiang, Y.; Fortner, J. D.; Yu, K.; Liao, P.; Liu, C. Formation and stability of NOM-Mn(III) colloids in aquatic environments. *Water Res.* **2019**, *149*, 190–201.

(36) Ma, D.; Wu, J.; Yang, P.; Zhu, M. Coupled manganese redox cycling and organic carbon degradation on mineral surfaces. *Environ. Sci. Technol.* **2020**, *54*, 8801–8810.

(37) Stuckey, J. W.; Goodwin, C.; Wang, J.; Kaplan, L. A.; Vidal-Esquivel, P.; Beebe, T. P.; Sparks, D. L. Impacts of hydrous manganese oxide on the retention and lability of dissolved organic matter. *Geochim. Trans.* **2018**, *19*, 6.

(38) Taujale, S.; Baratta, L. R.; Huang, J.; Zhang, H. Interactions in ternary mixtures of MnO₂, Al₂O₃, and natural organic matter (NOM) and the impact on MnO₂ oxidative reactivity. *Environ. Sci. Technol.* **2016**, *50*, 2345–2353.

(39) Estes, E. R.; Andeer, P. F.; Nordlund, D.; Wankel, S. D.; Hansel, C. M. Biogenic manganese oxides as reservoirs of organic carbon and proteins in terrestrial and marine environments. *Geobiology* **2016**, *15*, 158–172.

(40) Li, C.; Zhang, B.; Ertunc, T.; Schaeffer, A.; Ji, R. Birnessite-induced binding of phenolic monomers to soil humic substances and nature of the bound residues. *Environ. Sci. Technol.* **2012**, *46*, 8843–8850.

(41) Stone, A. T.; Morgan, J. J. Reduction and dissolution of manganese(III) and manganese(IV) oxides by organics. 1. Reaction with hydroquinone. *Environ. Sci. Technol.* **1984**, *18*, 450–456.

(42) Schwarzenbach, R. P.; Gschwend, P. M.; Imboden, D. M. *Environmental Organic Chemistry*, 2nd ed.; John Wiley & Sons, Inc.: Hoboken, New Jersey, 2003.

(43) Chen, M.; Hur, J. Pre-treatments, characteristics, and biogeochemical dynamics of dissolved organic matter in sediments: A review. *Water Res.* **2015**, *79*, 10–25.

(44) Huangfu, X.; Jiang, J.; Ma, J.; Liu, Y.; Yang, J. Aggregation kinetics of manganese dioxide colloids in aqueous solution: Influence of humic substances and biomacromolecules. *Environ. Sci. Technol.* **2013**, *47*, 10285–10292.

(45) Chorover, J.; Amistadi, M. K. Reaction of forest floor organic matter at goethite, birnessite and smectite surfaces. *Geochim. Cosmochim. Acta* **2001**, *65*, 95–109.

(46) Zhang, J.; McKenna, A. M.; Zhu, M. Macromolecular characterization of compound selectivity for oxidation and oxidative alterations of dissolved organic matter by manganese oxide. *Environ. Sci. Technol.* **2021**, *55*, 7741–7751.

(47) Graham, M. C.; Gavin, K. G.; Kirika, A.; Farmer, J. G. Processes controlling manganese distributions and associations in organic-rich freshwater aquatic systems: The example of Loch Bradan, Scotland. *Sci. Total Environ.* **2012**, *424*, 239–250.

(48) Komada, T.; Burdige, D. J.; Li, H.-L.; Magen, C.; Chanton, J. P.; Cada, A. K. Organic matter cycling across the sulfate-methane transition zone of the Santa Barbara Basin, California Borderland. *Geochim. Cosmochim. Acta* **2016**, *176*, 259–278.

(49) Poulin, B. A.; Ryan, J. N.; Nagy, K. L.; Stubbins, A.; Dittmar, T.; Orem, W.; Krabbenhoft, D. P.; Aiken, G. R. Spatial dependence of reduced sulfur in Everglades dissolved organic matter controlled by sulfate enrichment. *Environ. Sci. Technol.* **2017**, *51*, 3630–3639.

(50) McKenzie, R. M. The synthesis of birnessite, cryptomelane, and some other oxides and hydroxides of manganese. *Mineral. Mag.* **1971**, *38*, 493–502.

(51) *Report on Superior Bay*, St. Louis County, Minnesota, and Douglas County. Wisconsin E.P.A. Region V, 1975, No. 128.

(52) Wisconsin Department of Natural Resources. Lake Water Quality Database. <http://www.dnr.wi.gov/lakes/waterquality> (accessed June 8, 2020), 2021.

(53) Center for Limnology at Wisconsin-Madison, North Temperate Lakes U.S. Long-Term Ecological Research Network; National Science Foundation. <http://www.lter.limnology.wisc.edu> (accessed February 24, 2021), 2021.

(54) Weishaar, J. L.; Aiken, G. R.; Bergamaschi, B. A.; Fram, M. S.; Fujii, R.; Mopper, K. Evaluation of specific ultraviolet absorbance as an indicator of the chemical composition and reactivity of dissolved organic carbon. *Environ. Sci. Technol.* **2003**, *37*, 4702–4708.

(55) Helms, J. R.; Stubbins, A.; Ritchie, J. D.; Minor, E. C.; Kieber, D. J.; Mopper, K. Absorption spectral slopes and slope ratios as indicators of molecular weight, source, and photobleaching of chromophoric dissolved organic matter. *Limnol. Oceanogr.* **2008**, *53*, 955–969.

(56) De Haan, H.; De Boer, T. Applicability of light absorbance and fluorescence as measures of concentration and molecular size of dissolved organic carbon in humic Lake Tjeukemeer. *Water Res.* **1987**, *21*, 731–734.

(57) Peuravuori, J.; Pihlaja, K. Molecular size distribution and spectroscopic properties of aquatic humic substances. *Anal. Chim. Acta* **1997**, *337*, 133–149.

(58) Poulin, B. A.; Ryan, J. N.; Aiken, G. R. Effects of iron on optical properties of dissolved organic matter. *Environ. Sci. Technol.* **2014**, *48*, 10098–10106.

(59) Stumm, W.; Morgan, J. J. *Aquatic Chemistry: Chemical Equilibria and Rates in Natural Waters*, 3rd ed.; John Wiley & Sons, Inc.: United States of America, 1996.

(60) Stauffer, R. E. Cycling of manganese and iron in Lake Mendota, Wisconsin. *Environ. Sci. Technol.* **1986**, *20*, 449–457.

(61) Manceau, A.; Marcus, M. A.; Grangeon, S. Determination of Mn valence states in mixed-valent manganates by XANES spectroscopy. *Am. Mineral.* **2012**, *97*, 816–827.

(62) Dittmar, T.; Koch, B.; Hertkorn, N.; Kattner, G. A simple and efficient method for the solid-phase extraction of dissolved organic matter (SPE-DOM) from seawater. *Limnol. Oceanogr.: Methods* **2008**, *6*, 230–235.

(63) Koch, B. P.; Dittmar, T.; Witt, M.; Kattner, G. Fundamentals of molecular formula assignment to ultrahigh resolution mass data of natural organic matter. *Anal. Chem.* **2007**, *79*, 1758–1763.

(64) Maizel, A. C.; Remucal, C. K. The effect of advanced secondary municipal wastewater treatment on the molecular composition of dissolved organic matter. *Water Res.* **2017**, *122*, 42–52.

(65) Maizel, A. C.; Remucal, C. K. The effect of probe choice and solution conditions on the apparent photoreactivity of dissolved organic matter. *Environ. Sci. Processes Impacts* **2017**, *19*, 1040–1050.

(66) Charbonnet, J. A.; Duan, Y.; Sedlak, D. L. The use of manganese oxide-coated sand for the removal of trace metal ions from stormwater. *Environ. Sci. Water Res. Technol.* **2020**, *6*, 593–603.

(67) Park, J.-W.; Dec, J.; Kim, J.-E.; Bollag, J.-M. Effect of humic constituents on the transformation of chlorinated phenols and anilines in the presence of oxidoreductive enzymes or birnessite. *Environ. Sci. Technol.* **1999**, *33*, 2028–2034.

(68) Stone, A. T.; Morgan, J. J. Reduction and dissolution of manganese(III) and manganese(IV) oxides by organics. 2. Survey of the reactivity of organics. *Environ. Sci. Technol.* **1984**, *18*, 617–624.

(69) Wang, Y.; Stone, A. T. Reaction of Mn(III,IV) (hydr)oxides with oxalic acid, glyoxylic acid, phosphonoformic acid, and structurally-related organic compounds. *Geochim. Cosmochim. Acta* **2006**, *70*, 4477–4490.

(70) Gustafsson, J. P. *Visual MINTEQ, 3.1*; KTH: Sweden, 2020.

(71) Li, Z.; Shakiba, S.; Deng, N.; Chen, J.; Louie, S. M.; Hu, Y. Natural organic matter (NOM) imparts molecular-weight-dependent steric stabilization or electrostatic destabilization to ferrihydrite nanoparticles. *Environ. Sci. Technol.* **2020**, *54*, 6761–6770.

- (72) Huang, J.; Zhong, S.; Dai, Y.; Liu, C.-C.; Zhang, H. Effect of MnO_2 phase structure on the oxidative reactivity toward bisphenol A degradation. *Environ. Sci. Technol.* **2018**, *52*, 11309–11318.
- (73) Tripathy, S. S.; Kanungo, S. B. Adsorption of Co^{2+} , Ni^{2+} , Cu^{2+} and Zn^{2+} from 0.5 M NaCl and major ion sea water on a mixture of δ - MnO_2 and amorphous FeOOH . *J. Colloid Interface Sci.* **2005**, *284*, 30–38.
- (74) Balgooyen, S.; Remucal, C. K.; Ginder-Vogel, M. Identifying the mechanisms of cation inhibition of phenol oxidation by acid birnessite. *J. Environ. Qual.* **2020**, *49*, 1644–1654.
- (75) Gomez-Saez, G. V.; Pohlbeln, A. M.; Stubbins, A.; Marsay, C. M.; Dittmar, T. Photochemical alteration of dissolved organic sulfur from sulfidic porewater. *Environ. Sci. Technol.* **2017**, *51*, 14144–14154.
- (76) Raeke, J.; Lechtenfeld, O. J.; Wagner, M.; Herzsprung, P.; Reemtsma, T. Selectivity of solid phase extraction of freshwater dissolved organic matter and its effect on ultrahigh resolution mass spectra. *Environ. Sci. Processes Impacts* **2016**, *18*, 918–927.
- (77) Lever, J.; Krzywinski, M.; Altman, N. Principal component analysis. *Nat. Methods* **2017**, *14*, 641–642.
- (78) Arnold, W. A.; Oueis, Y.; O'Connor, M.; Rinaman, J. E.; Taggart, M. G.; McCarthy, R. E.; Foster, K. A.; Latch, D. E. QSARs for phenols and phenolates: Oxidation potential as a predictor of reaction rate constants with photochemically produced oxidants. *Environ. Sci. Processes Impacts* **2017**, *19*, 324–338.
- (79) Davi, M. L.; Gnudi, F. Phenolic compounds in surface water. *Water Res.* **1999**, *33*, 3213–3219.
- (80) McCabe, A. J.; Arnold, W. A. Reactivity of triplet excited states of dissolved natural organic matter in stormflow from mixed-use watersheds. *Environ. Sci. Technol.* **2017**, *51*, 9718–9728.
- (81) Zhang, J.; McKenna, A. M.; Zhu, M. Macromolecular characterization of compound selectivity for oxidation and oxidative alterations of dissolved organic matter by manganese oxide. *Environ. Sci. Technol.* **2021**, *55*, 7741–7751.
- (82) Wu, P.; Fu, Q.-L.; Zhu, X.-D.; Liu, C.; Dang, F.; Müller, K.; Fujii, M.; Zhou, D.-M.; Wang, H.-L.; Wang, Y.-J. Contrasting impacts of pH on the abiotic transformation of hydrochar-derived dissolved organic matter mediated by δ - MnO_2 . *Geoderma* **2020**, *378*, 114627.
- (83) Canonica, S.; Tratnyek, P. G. Quantitative structure-activity relationships for oxidation reactions of organic chemicals in water. *Environ. Toxicol. Chem.* **2003**, *22*, 1743–1754.
- (84) Lee, Y.; von Gunten, U. Quantitative structure-activity relationships (QSARs) for the transformation of organic micro-pollutants during oxidative water treatment. *Water Res.* **2012**, *46*, 6177–6195.
- (85) Bulman, D. M.; Mezyk, S. P.; Remucal, C. K. The impact of pH and irradiation wavelength on the production of reactive oxidants during chlorine photolysis. *Environ. Sci. Technol.* **2019**, *53*, 4450–4459.
- (86) Tentscher, P. R.; Bourgin, M.; von Gunten, U. Ozonation of *para*-substituted phenolic compounds yields *p*-benzoquinones, other cyclic α,β -unsaturated ketones, and substituted catechols. *Environ. Sci. Technol.* **2018**, *52*, 4763–4773.
- (87) Li, Y.; Harir, M.; Uhl, J.; Kanawati, B.; Lucio, M.; Smirnov, K. S.; Koch, B. P.; Schmitt-Kopplin, P.; Hertkorn, N. How representative are dissolved organic matter (DOM) extracts? A comprehensive study of sorbent selectivity for DOM isolation. *Water Res.* **2017**, *116*, 316–323.
- (88) Wang, Q.; Yang, P.; Zhu, M. Structural transformation of birnessite by fulvic acid under anoxic conditions. *Environ. Sci. Technol.* **2018**, *52*, 1844–1853.
- (89) Wang, Q.; Yang, P.; Zhu, M. Effects of metal cations on coupled birnessite structural transformation and natural organic matter adsorption and oxidation. *Geochim. Cosmochim. Acta* **2019**, *250*, 292–310.
- (90) Amiri, F.; Börnick, H.; Worch, E. Sorption of phenols onto sandy aquifer material: The effect of dissolved organic matter (DOM). *Water Res.* **2005**, *39*, 933–941.